Progress Report of HINDAS Work Package 6
(High- and Intermediate-Energy Nuclear Data for Accelerator-Driven Systems)

Production of residual nuclei in the spallation of ^{238}U by 1 GeV protons and 2 GeV deuterons, measured in inverse kinematics

M. Bernas[1)], E. Casarejos[2)], J. Pereira[2)], M. V. Ricciardi[3)], J. Taïeb[1)], P. Armbruster[3)], J. Benlliure[2)], A. Boudard[4)], S. Czajkowski[5)], T. Enqvist[6)], R. Legrain[4)], S. Leray[4)], B. Mustapha[1)], M. Pravikoff[5)], F. Rejmund[1)], K.-H. Schmidt[3)], C. Stéphan[1)], L. Tassan-Got[1)], C. Volant[4)], W. Wlazło[4)]

[1)]IPN Orsay, IN2P3, F-91406 Orsay, France
[2)]University of Santiago de Compostela, E-15706 Santiago de Compostela, Spain
[3)]GSI, Planckstraße 1, D-64291 Darmstadt, Germany
[4)]DAPNIA/SPhN CEA/Saclay, F-91191 Gif sur Yvette, France
[5)]CENBG, IN2P3, F-33175 Gradignan, France
[6)]University of Jyväskylä, 40351 Jyväskylä, Finland

September 2002

Progress Report of HINDAS Work-Package 6 [*]
(High- and Intermediate-Energy Nuclear Data for Accelerator-Driven Systems)

Production of residual nuclei in the spallation of ^{238}U by 1 GeV protons and 2 GeV deuterons, measured in inverse kinematics[†]

M. Bernas, E. Casarejos, J. Pereira, M. V. Ricciardi, J. Taïeb,
P. Armbruster, J. Benlliure, A. Boudard, S. Czajkowski, T. Enqvist, R. Legrain,
S. Leray, B. Mustapha, M. Pravikoff, F. Rejmund, K.-H. Schmidt, C. Stéphan,
L. Tassan-Got, C. Volant, W. Wlazło

September 2002

1. Introduction

Since some years, spallation reactions have gained a renewed interest for several reasons. On the one hand, they are planned to be used in the so-called Accelerator Driven System as an intense neutron source. On the other hand, spallation reactions lead to the production of unstable nuclei. This reaction is actually exploited in ISOL-type facilities.

Therefore, a campaign of measurements of spallation residues started at GSI, taking advantage of the use of the inverse kinematics. The results obtained in the spallation of gold and lead have already been published extensively [1, 2, 3, 4, 5]. In both cases, the projectile energy was close or equal to 1 GeV per nucleon in order to mimic the spallation of a heavy nucleus by 1 GeV protons and 2 GeV deuterons, respectively. These measurements are supposed to give high constraints for the codes aimed for designing accelerator-driven systems (ADS) and new facilities for the production of Radioactive Nuclear Beams. They also give some clear hints for a better understanding of the spallation reaction.

This paper focuses on the production of residues in the spallation of ^{238}U. Due to the high fissility of the reaction products, great part of them fission, leading to a production of a large number of nuclides in the mid-mass region. But also the production of heavy residues is conditioned by the fission of isotopes during the evaporation phase. Therefore, surprisingly, the measurement of evaporation residues is of the highest interest for testing the fission probability estimated by the de-excitation codes. This problem is connected to some fundamental questions on the evolution of the level density or the barrier height with increasing excitation energy. We are also able to study the dissipation in the fission process. All those are still open questions.

The measurements of evaporation and fission residues have started since the proton accelerators became available in the 50's. For 40 years, production of residues was measured using chemical and/or spectroscopic methods. In the 90's, the GSI gave birth to a new generation of machines, coupling an intense and powerful heavy-ion accelerator and a precise recoil spectrometer (the FRS [6]). The installation of a cryogenic hydrogen target [7] permitted to start the campaign of measurement of spallation-residue cross sections. We could detect, identify unambiguously and analyse several hundreds of isotopes before radioactive disintegration

[*] Lead contractor of HINDAS WP6: K.-H. Schmdit, GSI
[†] This report is available in the WEB: (http://www-wnt.gsi.de/kschmidt/publica.htm, Internal Reports)

with an accuracy in the order of 10% to 15% in most cases. This strongly contrasts with the scarce and usually cumulative cross sections obtained with other techniques. The high efficiency of the spectrometer coupled to the very short time-of-flight (about 300ns) contributes strongly to the quality of our results.

In this paper, we report on the first systematic study of nuclide production in isotopic chains from nitrogen (Z=7) to uranium (Z=92) [8, 9, 10, 11, 12]. In the second section, we present some characteristics of the experimental set up and the analysis techniques. In the third and in the forth part, we report on the obtained cross sections and kinematical properties of the studied nuclei, respectively. In the last section, we discuss the results and compare them to data obtained previously with conventional techniques.

2. The experiment

The experimental set up has already been described extensively in other publications using gold and lead projectiles [1, 2, 3, 4, 5]. In the present chapter, we give an overview of the main aspects of the experiment and stress the improvements, which were necessary for this specific measurement.

The 1 A GeV ^{238}U beam, produced by the synchrotron SIS of GSI interacted with a liquid target of ^{1}H and ^{2}H, respectively. The products of the reaction are separated and analysed by the recoil spectrometer FRS. The experimental apparatus is shown Figure 1. The two-stage fragment separator allows a full identification in nuclear charge, Z, and mass number, A, of the fragment. Moreover, the recoil momentum is also provided. The reaction products suffer a first magnetic selection; then, they are slowed down in a layer of matter situated at the intermediate focal plane. In the case of the heaviest residues, this is a thick passive energy degrader; for the lighter residues it is a scintillation detector, only. A second magnetic selection is finally applied. The time-of-flight is measured between both image planes thanks to two plastic scintillation detectors. Moreover, two multiply sampling ionisation chambers (MUSIC) give a couple of energy-loss signals. They are placed at the very end of the spectrometer. Therefore, for each ion passing through we obtain two magnetic rigidities, a time-of-flight and a couple of energy-loss measurements.

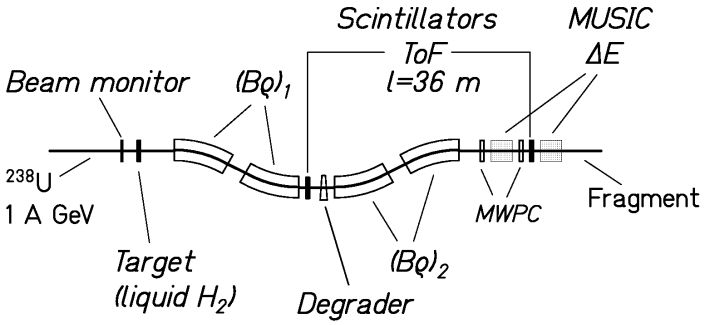

Figure 1 : Schematic drawing of the fragment separator (FRS) with its most important components. The primary beam of ^{238}U enters from the left.

2.1. The energy loss in the degrader

The nuclear-charge determination of the heaviest residues is certainly the most challenging problem that we had to face. It was a special aim of the experiment to improve the nuclear-charge resolution, previously obtained [13, 14]. This is especially true for the heaviest elements (the actinides) for which the separation is the most difficult. This high-resolution nuclear-charge determination could be obtained through a multi-fold measurement, as shown in Figure 2. First of all, we remind that a thick energy degrader is placed at the intermediate image plane (see Figure 1). This passive component of the set up indirectly helps determining the nuclear charge. Actually, the magnetic rigidities are measured before and after the ions pass through the degrader. The difference of those two quantities is linked with the momentum (and energy) loss within the degrader plate, following the relation:

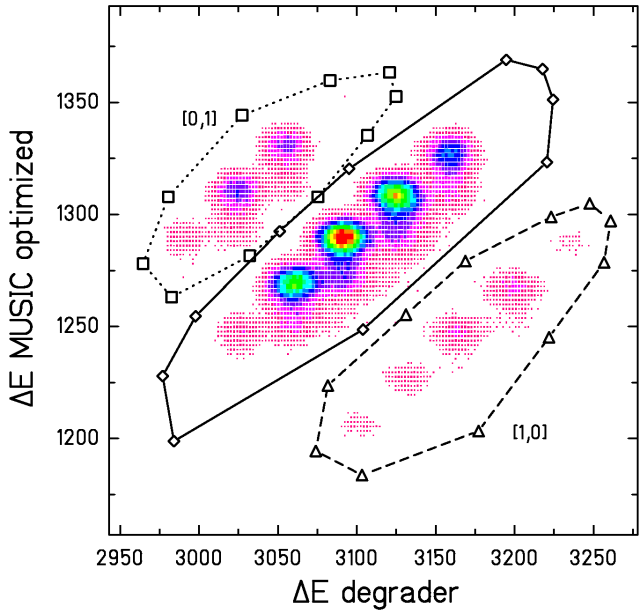

Figure 2 : Separation of nuclear charges around Z = 90 and elimination of different ionic charge states. The ions which do not change their charge state all along the separator are inside the full contour line. The ions which capture one electron in the degrader section are inside the dotted contour line, while the ions which loose one electron in the degrader section are inside the dashed contour line. The most intense peak corresponds mostly to fully stripped thorium ions.

$$(B\rho)_1 - (B\rho)_2 = p_1/q_1 - p_2/q_2 \qquad (1)$$

where $(B\rho)_1$ and $(B\rho)_2$ are the magnetic rigidities, p_1 and p_2 are the momenta, and q_1 and q_2 are the ionic charge states of the ion before and after the degrader, respectively. Assuming, for the moment that the ions are fully stripped:

$$q_1 = q_2 = Z \qquad (2)$$

the $B\rho$ difference provides an estimate of the energy loss within the degrader. Nuclei for which the condition (2) is not fulfilled will be rejected in the analysis process as shown in the following section.

2.2. The nuclear charge resolution

The best charge resolution is obtained correlating, on one hand, both signals coming from the ionisation chambers, and, on the other hand, the $B\rho$-difference measurement presented in the previous section. The signals provided by the ionisation chambers are combined in order to get a single optimised quantity. A bi-dimensional plot illustrating the correlation between the so-called "energy loss in the degrader" and the optimised energy loss in the MUSIC chambers is shown in Figure 2.

Figure 2 is obtained for a specific setting. This means a specific set-up of the various magnetic fields. The number of different isotopes passing through the FRS depends on the $B\rho$ acceptance of the spectrometer and on the thickness of the energy degrader. Therefore, a number of several hundred settings was necessary for providing the whole set of data presented in this paper.

For the heaviest nuclei, the appearance of different ionic charge states represents a particular difficulty. Three different regions can be observed on Figure 2. They correspond to three different charge-state combinations. The central zone includes the fully stripped ions and the H-like ones. What is important is that the ions, in this region are bare or H-like all along their trajectory. That is, they do not change their charge state between the first and the second half of the FRS.

Actually, the ions are fully bare after the collision most of the time at 1 GeV per nucleon. However, the probability that a heavy ion like the projectile carries one electron is not negligible (around 10%). When arriving at S2, the ions pass through a number of different layers of matter, namely, the scintillation detector and, in part of the settings, the degrader plate. Traversing those materials, the ions successively gain and lose electrons alternating between bare and H-like status. In most cases, they leave the intermediate image plane bare (due to the high kinetic energy). Finally the probability that the ion is hydrogen-like all along its trajectory is rather low, even for the heaviest fragments, compared to the most probable situation (bare over the whole flight-path). The contamination of the central zone on Figure 2 due to the ions carrying one electron in **both** sections is estimated to be at most in the order of 1 to 2% depending on the nuclear charge of the ion (the higher is the charge the higher is the contamination). This contamination is neglected in the analysis.

The two other zones (labelled [1,0] and [0,1]) are to be associated to the ions carrying 1 electron in the first (region [1,0]) or second (region [0,1]) section of the FRS, being bare in the other part of the spectrometer. Only the central region in Figure 2 is being analysed for getting the cross sections. Neglecting the contamination due to ions which carry one electron in both sections, we ensure that all ions are fully stripped gating on the central region. Therefore, the following condition is valid:

$$q_1 = q_2 = Z \tag{3}$$

Every spot within the selected region corresponds to a common value of the energy loss in the degrader and in the MUSIC chambers. This correlation is the best way for disentangling the various nuclear charges traversing the spectrometer. Thus, each spot corresponds to a specific nuclear charge. The charge separation is seen to be rather good. Projecting the central window on an inclined axis, we obtain a curve whose peak-to-valley ratio varies between 10 and 20

(the latter value for the heaviest elements). It is the first time that such a high nuclear-charge resolution could be obtained in an in-flight-separation experiment, exploring elements up to uranium.

After selection of a specific spot (and thus a specific nuclear charge) in the central window, the mass spectrum is obtained thanks to the $B\rho$ and velocity measurements in the second section of the FRS according to the following expression:

$$A = \frac{Z \cdot e \cdot (B\rho)_2}{m_0 \cdot c \cdot \beta_2 \gamma_2} \tag{4}$$

where β_2 and γ_2 are the reduced velocity and Lorentz parameter in the second half of the spectrometer. They are deduced from the ToF measurement. Z is the nuclear charge and e, m_0 and c are the charge of the electron, the mass unit, and the velocity of light, respectively. The following two-dimensional plot (Figure 3) of the mass versus the position at the intermediate image plane illustrates the high mass resolution. This precise mass measurement is achieved from a high-quality ToF resolution (130 ps) and a long flight path. The consecutive mass resolution is

$$A/\Delta A = 300 \text{ (FWHM)} \tag{5}$$

Figure 3 shows that many isotopes are cut at the intermediate image plane due to the limited $B\rho$ acceptance of the spectrometer. Therefore, a number of 70 settings was necessary for covering the whole range in magnetic rigidity of the heavy spallation-evaporation residues. The broadening of the horizontal distribution at S2 reflects the extension of the velocity distribution mainly due to the nuclear reaction.

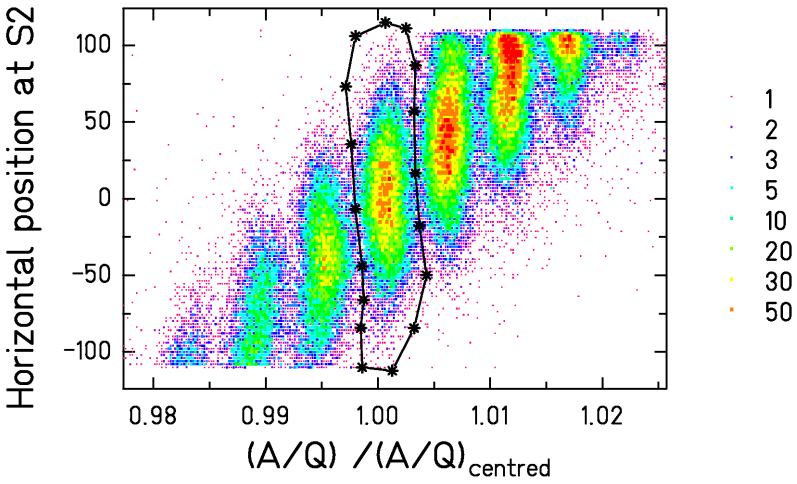

Figure 3 : Two-dimensional cluster plot of the horizontal position at the central image plane (S2) versus the A/Q value, normalized to the one of the centred nucleus. The data are recorded in the reaction of 1 *A* GeV ^{238}U in the hydrogen target in one specific setting of the fragment separator. The contour line indicates the centred nucleus, ^{192}Pb. The colour code gives the counts per channel.

The lighter nuclei, which are produced in spallation-fission rections, are characterised by very broad velocity distributions. Therefore, a large number of setting had to be combined in order to reconstruct their complete velocity distributions. This is illustrated by the two-dimensional

representation for the iron isotopes shown in Figure 4. In contrast to the heavier nuclei, the data of the different settings for Z < 30 did not overlap due to lack of beam time. Nevertheless, the data give a rather complete impression on the characteristics of the velocity distributions of the reaction products. The most important production at about +1.4 cm/ns and –1.8 cm/ns result from fission in the hydrogen target. Production at velocities close to the beam result from reactions in the titanium windows of the target container.

The production rates could be obtained for about 350 spallation-evaporation residues ranging from uranium to tungsten, giving a total number of 1206 individual values, including the fission residues, in the proton-induced reaction. In the deuteron-induced reaction a total number of 1303 individual production rates were determined. For getting cross sections, losses due to non-fully stripped ions and nuclear reactions at S2 are accounted for. The losses are estimated theoretically and these evaluations are confirmed with online measurements. During the experiment, the number of incoming projectiles is recorded by a beam monitor, a secondary electron chamber [15]. The thickness of the H_2 liquid target has been determined experimentally previously [16]. The contribution, to the production rate, due to the windows of the target was measured during the beam time using an empty target. This part is measured to lie between 5% and 15% of the total production rate. This contribution was corrected for. More details about the applied correction procedure are given in ref. [4].

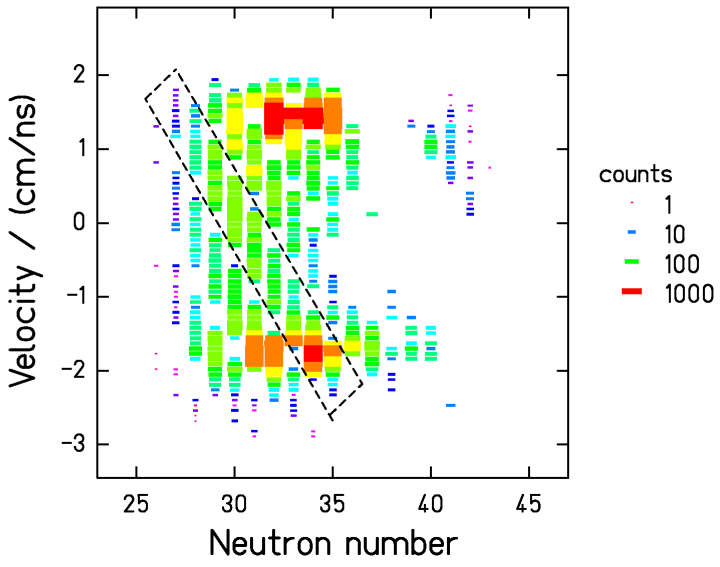

Figure 4 : Two-dimensional cluster plot of the velocity distributions of iron isotopes produced by 1 *A* GeV ^{238}U in the hydrogen target. The velocity is given in the frame of the beam. The colour code gives the number of counts per channel. The data recorded in one setting of the fragment separator are marked by the dashed contour line. Although the data of the different settings do not overlap, the data give a complete impression on the velocity patterns of the different isotopes. One setting of the regular pattern is missing, because it was too close to the magnetic rigidity of the primary beam.

Actually, the region around Z = 60 to Z = 70 is only slightly populated, being situated in the low-mass tails of the spallation-evaporation and in the high-mass tails of the spallation-fission regions. In this region, we could not disentangle the fission fragment from the evaporation residues, and we noticed that both were present in this charge region. Therefore, we chose not to produce this part of the data and restrict ourselves to the nuclei identified as pure evaporation residues or fission residues, respectively. The gap between spallation-evaporation and

spallation-fission residues is different for the two systems since spallation-evaporation residues extend to lower masses for the deuteron-induced reaction.

Finally, we are able to give a total of 2509 individual production cross sections for the two systems studied. For each of these nuclei, we also measured the recoil velocity distribution.

3. Results

3.1 Measured cross sections

Figure 5 shows the measured isotopic cross sections for all elements ranging from fluorine (Z=9) to uranium (Z=92). They vary from about 10 μb to 100 mb. The fluctuations within the isotopic distributions are rather low, illustrating the high quality of the data. However a few dips can be observed for elements from thorium to astatine in the ^{238}U+^{1}H system (see Figure 5). Actually, the very short time of flight of the ions (150 ns eigen-time) authorises the measurement of the production cross sections for most of the isotopes, namely when the radioactive-decay period is much longer than the time-of-flight of the ions. Several isotopes characterized by a number of 128 neutrons (position of the dips) decay by α emission toward the 126-neutron shell. The decay period of those isotopes is of the order of the time-of-flight through the FRS. Therefore, part of the production is lost before being analysed and identified. Moreover, when the decay occurs at the very beginning of the flight path, the ion is "seen" as the daughter nucleus. This effect causes the slight "hump" that can be observed for ^{211}As. The apparent over-production of this isotope is due to the very fast decay of the ^{215}Fr (T_{α}=90 ns to be compared to the ToF=150 ns eigentime). It is not simple to correct for this effect since isomers are populated in this mass region. Moreover, the branching ratio and associated decay period are up to now unknown. A couple of isotones with a number of 129 neutrons are also concerned. Mainly ^{214}At suffers from the very fast decay. The very fast decay of a few nuclei preventing from giving true cross sections demonstrates the high quality of our data. This ensures that the uncertainty is as low as claimed since effects of 10% to 20% can be observed. Moreover, we guarantee that the mass and charge identification is correct. For the system ^{238}U + ^{2}H, a correction for losses due to in-flight decay has been applied.

We observed, for the first time, the isotope ^{235}Ac, which corresponds to the 3-proton removal channel. 150 events were unambiguously recorded. This points out again [17] that the so-called cold fragmentation is a favourable path for producing heavy exotic neutron-rich nuclei.

These nuclide cross sections are represented on a chart of the nuclides for the two systems investigated on Figure 6 and Figure 7.

The data represent the cross sections obtained in a target of 87.3 mg/cm^2 hydrogen and 208 mg/cm^2 deuterium, respectively. While the contribution of the target-container windows is subtracted, they are not corrected for secondary reactions inside the production target. To perform this correction will be a major task, because it requires a very accurate reproduction of all nuclide reaction cross sections starting from each of the reaction products with a fast nuclear-reaction code. The strong fission competition complicates this task considerably, compared to the corresponding procedure applied to the ^{208}Pb + ^{1,2}H systems [4, 5]. This code is actually being developed. The data on the spallation of gold and lead measured previously give the necessary constraints for the development of this code. This correction is expected to influence the lower mass range of the spallation-evaporation residues and the most neutron-

deficient isotopes of the spallation-fission residues. It is expected to be similar to the correction applied to the lead systems, see refs. [4, 5].

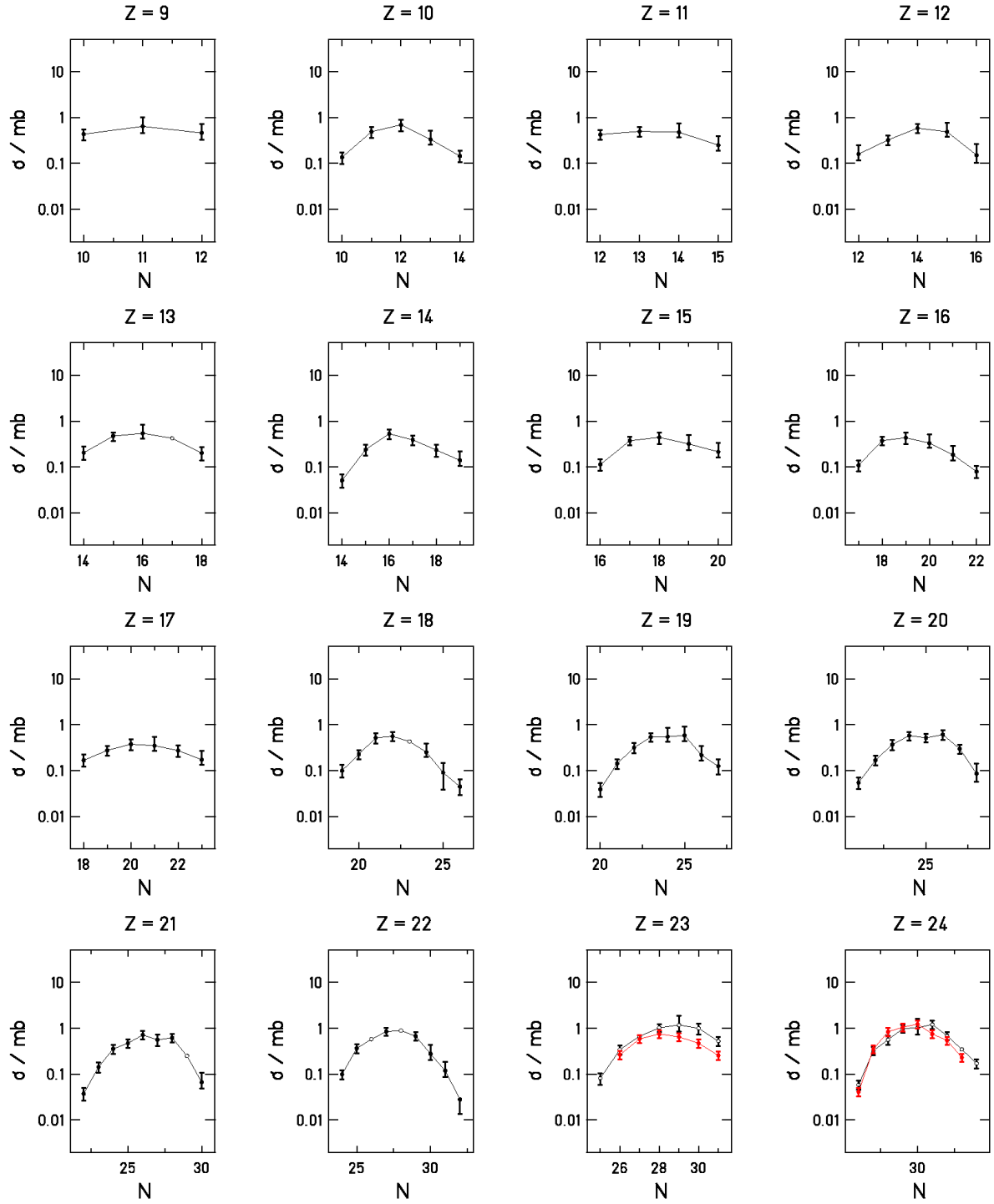

Figure 5 : Isotopic production cross sections for more than 1000 nuclides from the spallation of ^{238}U by 1 GeV protons (black symbols) and by 2 GeV deuterons (red symbols). The measurement was performed in inverse kinematics. The open symbols given for some isotopes of the lighter elements show estimations based on the systematics of the general behaviour.

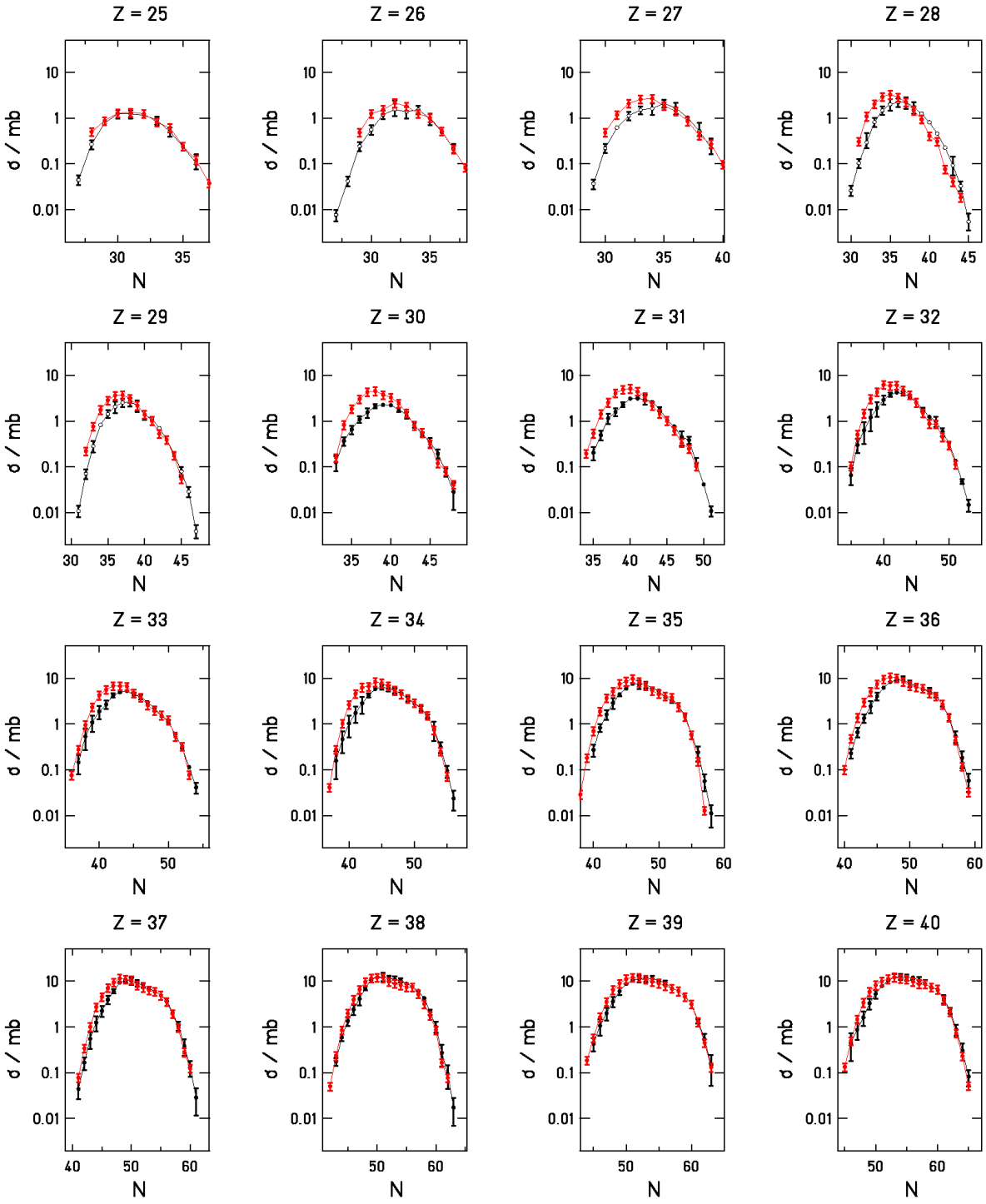

Figure 5 continued

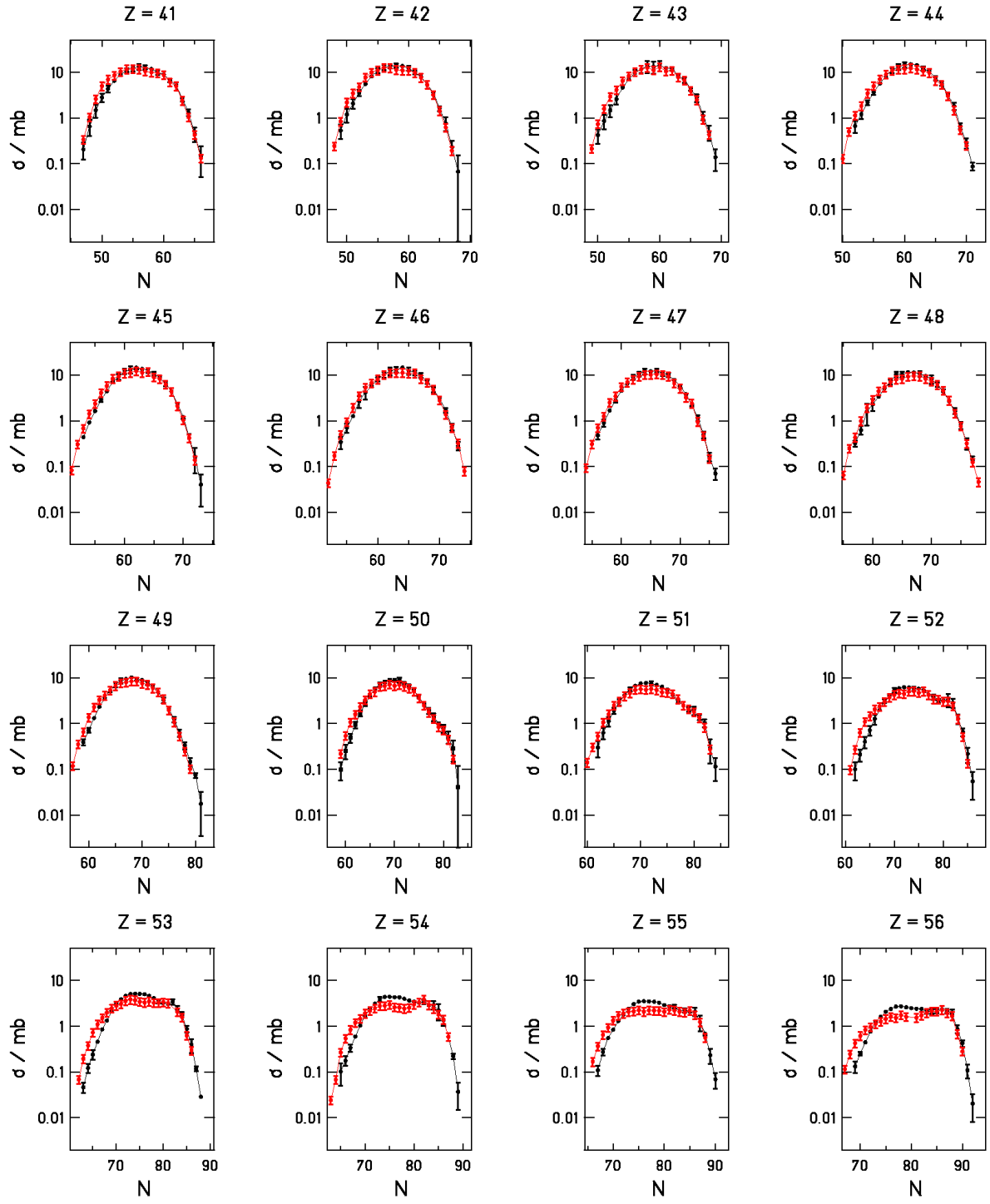

Figure 5 continued

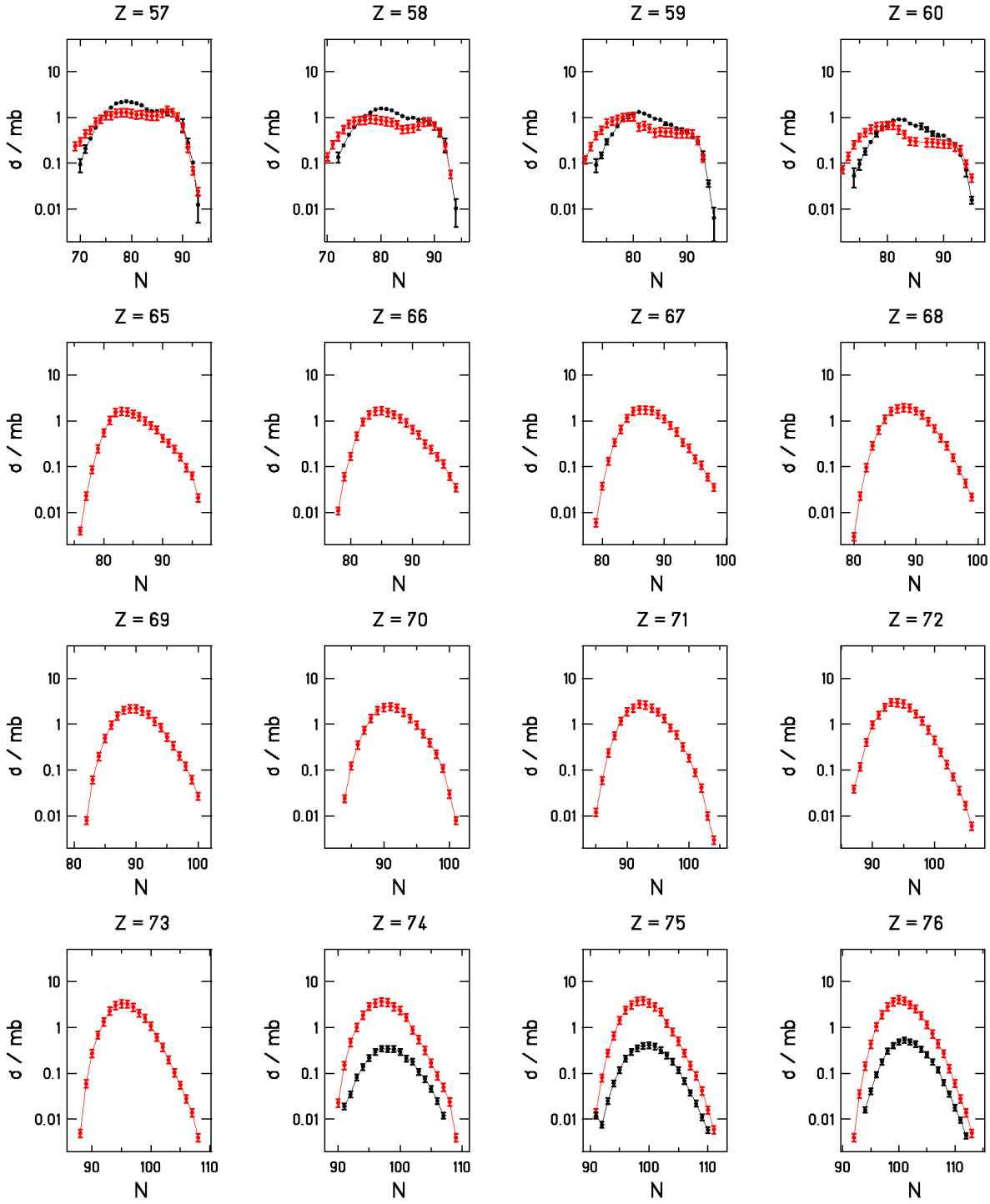

Figure 5 continued

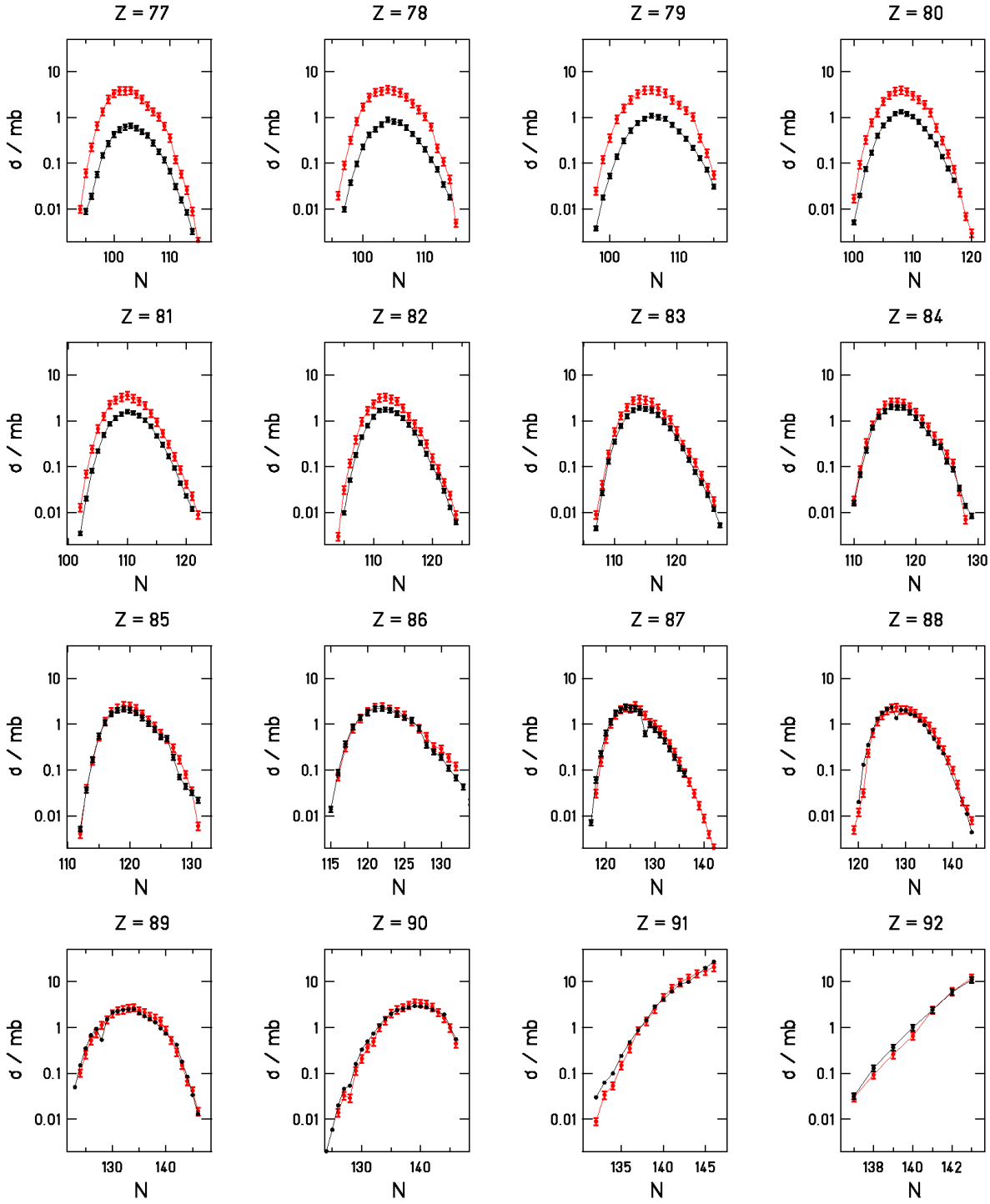

Figure 5 continued

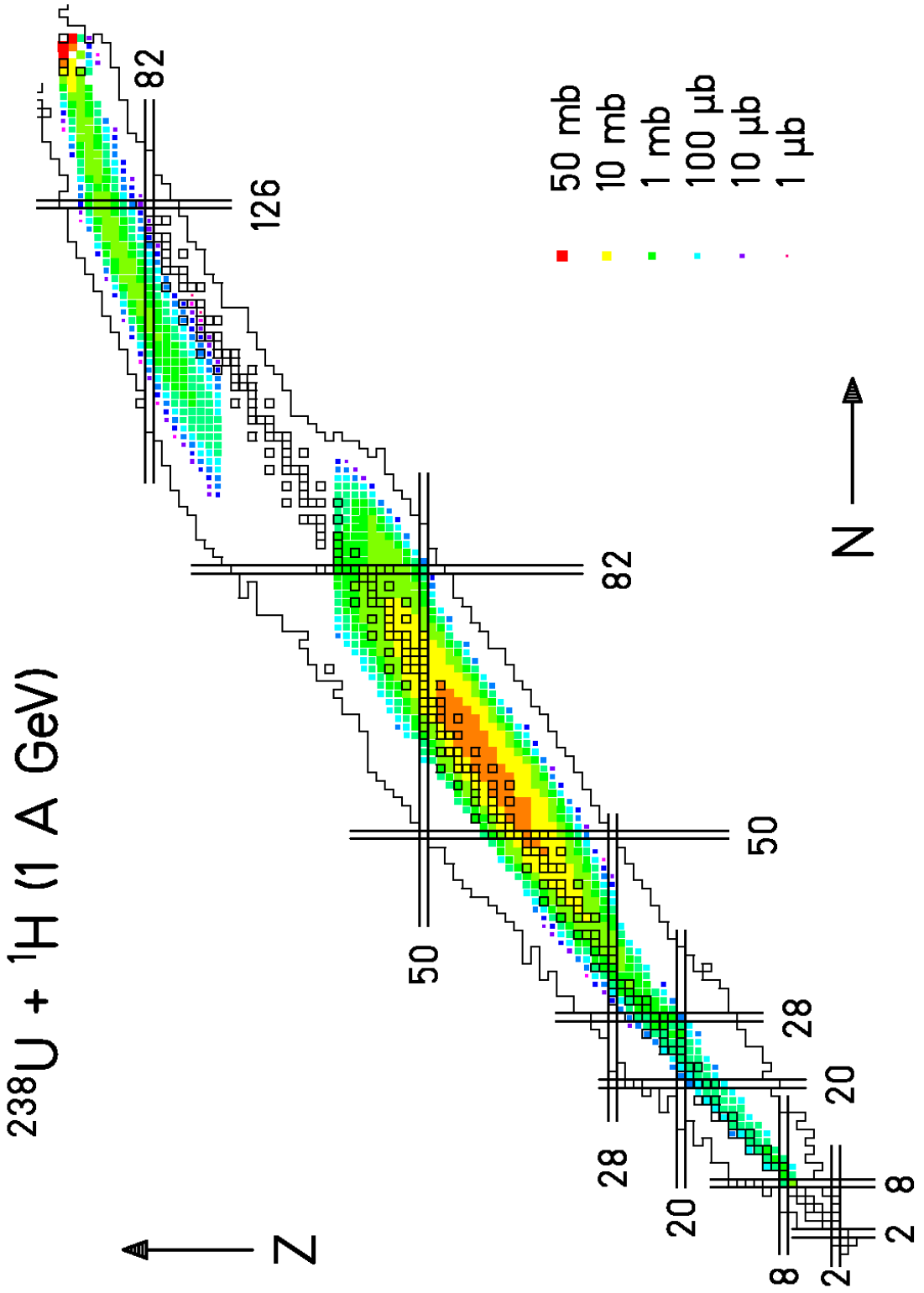

Figure 6 : Nuclide cross sections of the reaction $^{238}U + ^{1}H$ at 1 A GeV presented on the chart of the nuclides.

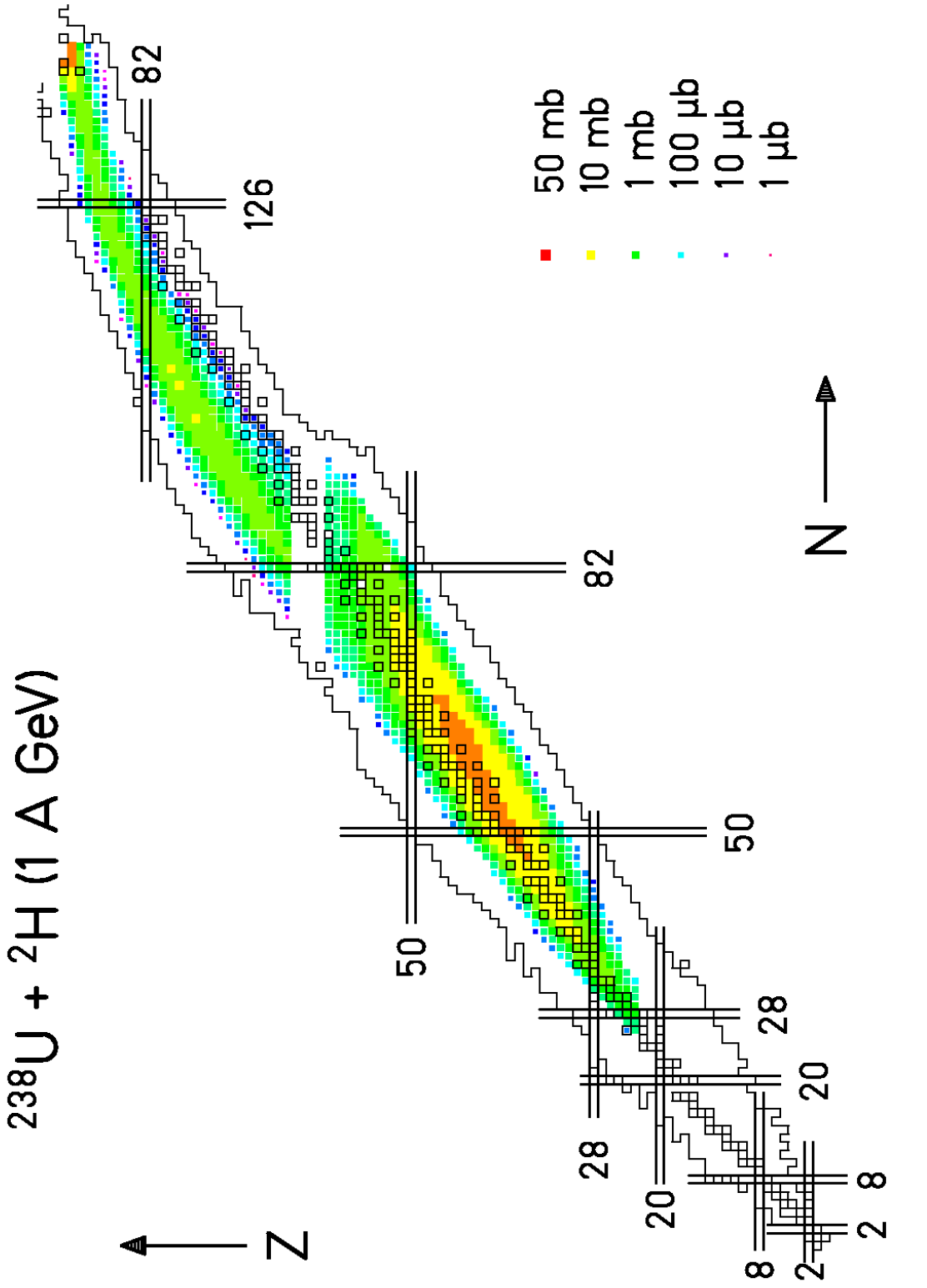

Figure 7 : Nuclide cross sections of the reaction $^{238}U + ^{2}H$ at 1 A GeV presented on the chart of the nuclides.

Thanks to the measurement of the full isotopic chains, we are able to produce sensible isobaric cross sections, this means, cross sections summed up over the full isobaric chains. The associated plot is reproduced in Figure 8, which includes two other distributions. Thus, we show, on the same graph, the isobaric cross sections obtained by the same collaboration, following a similar procedure, with gold projectiles (^{197}Au) at 800 MeV per nucleon [1] and lead (^{208}Pb) at 1 GeV per nucleon [4]. The isobaric cross section is figured as a function of the mass loss.

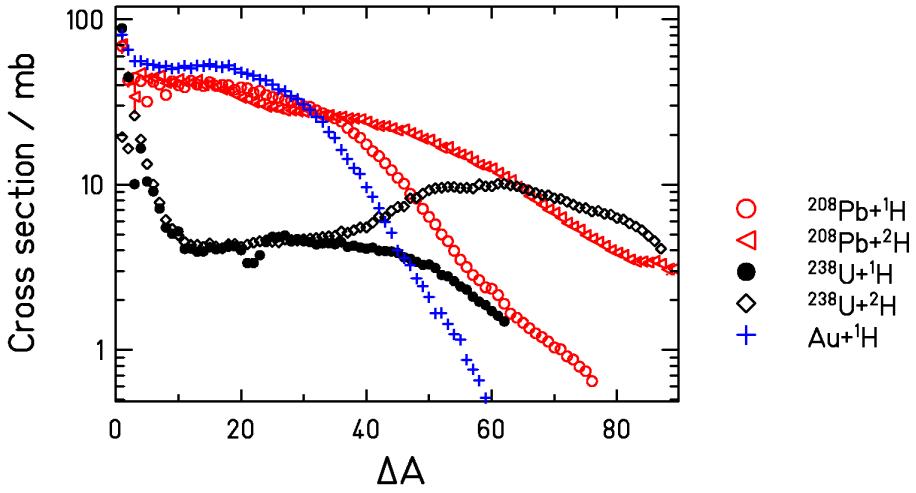

Figure 8 : Isobaric cross sections as a function of mass loss for three reactions. The full symbols mark the system ^{238}U + ^{1}H and the diamonds mark the system ^{238}U + ^{2}H at 1 *A* GeV, studied in this work, the crosses result from the reaction ^{197}Au + ^{1}H at 800 *A* MeV [1], the open circles represent the system ^{208}Pb + ^{1}H at 1 *A* GeV [4], and the triangles represent the system ^{208}Pb + ^{2}H at 1 *A* GeV [5].

As far as low-fissility nuclei are concerned (gold and lead), the trends are very much similar. The main difference can be observed for the lowest masses. The lighter evaporation residues are less produced in the gold experiment. The explanation appears clearly when considering the difference in term of projectile energy. Within the frame of a two-stage model, the first phase of the interaction leads to the production of an excited nucleus. The excitation spectrum depends on the energy of the projectile. The fastest projectile leads to the highest excitation energy (as far as the so-called limiting-fragmentation regime is not reached) inducing the longest evaporation chain and producing the lightest evaporation residues. The height of both distributions (spallation of gold and lead) is similar for the heaviest residues.

Concerning the spallation of uranium, the shape and the height of the isobaric distributions are pretty much different. As far as U+^{1}H data is concerned, we notice a slight dip for mass losses close to 22. This depression is due to the very fast alpha decay of N = 128 isotones toward the 126-neutron shell earlier described in the paper. The affected data may be evaluated using the isotopic chains which are accurately measured. That evaluation was done for U+ ^{2}H data, and we can see that the dip is not longer present. Moreover, below a loss of 60 mass units, the cross sections are notably lower in the uranium case than obtained for the two other experiments. The effect is stronger for the heaviest fragments. The explanation lies in the strong depletion effect of the fission process for actinide nuclei. During the evaporation phase, the fission probability is much higher for actinides than for rare-earth nuclei, which are involved in the spallation of gold or lead. Thus, in the case of uranium, the production of evaporation residues is paradoxically very much influenced by the fission mechanism. This observation is

confirmed by comparing the isotopic cross section for production of isotopes of the projectile element in the uranium, lead, and gold experiments. The cross sections are plotted in Figure 9 as a function of the neutron loss for all three experiments. The distributions appear very different. As the cross sections are similar for the one-neutron removal channel, they rapidly diverge when increasing the number of lost neutrons. A longer de-excitation chain produces the more neutron-deficient isotopes. Two effects contribute to the fast decrease of the production cross section with increasing neutron loss. First-of-all, the longer is the de-excitation chain the higher is the cumulated fission probability. Obviously, longer evaporation chains produce the lighter uranium isotopes. Moreover, the fission barriers decrease for the more neutron-deficient nuclei, favouring again the fission process relative to the evaporation of particles. Thus, as the neutron-rich part of the isotopic distribution is not much affected by the fission mechanism, the neutron-deficient region is strongly depopulated. Close to the projectile, the length of the isotopic chains is notably shorter in the uranium case than in the other ones. An interesting observation is that in the same experiment we produce low and highly excited very fissile pre-fragments. Therefore, these data contain relevant information about the competition between fission and evaporation in a wide range of fissility and excitation.

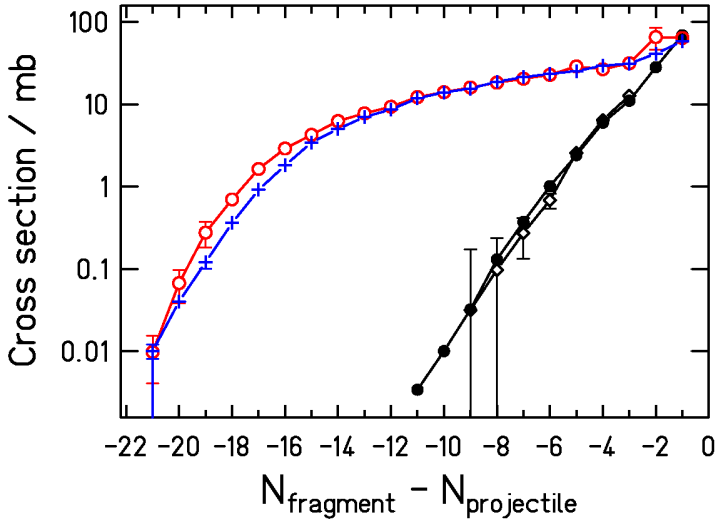

Figure 9 : Isotopic cross section for production of projectile isotopes in the uranium, lead, and gold experiments. Symbols are the same as in figure 8. The cross sections are plotted as a function of the neutron number relative to the projectile.

In Figure 9 we also compare the uranium productions from proton- and deuteron-induced reactions on ^{238}U: they are about the same. This is the case for most of the isotopes of elements close to the projectile. That can be understood considering that those isotopes come from the most peripheral, thus less energetic, collisions. Due to the wide spatial distribution of the deuteron, many collisions would imply the impact of a single nucleon: proton and deuteron reactions would produce the same result. Additionally, no differences between proton and neutron collisions were found.

Coming back to the isobaric cross sections shown in Figure 8, the first qualitative observation is that the distributions associated to the lead and uranium experiments join for mass losses close to 60. The depletion effect observed on the cross section for the heaviest nuclei seems to vanish for the lightest evaporation residues. In the two-stage model, this observation seems surprising. Actually, the first step of the reaction leads to the production of an excited so-called pre-fragment. According to calculations with intra-nuclear cascade codes, the mass and

nuclear charge of this nucleus is close to the one of the projectile (only 5 to 10 nucleons could be removed). Therefore, the light evaporation residues (for instance with a mass loss equal to 60 compared to the projectile) are consecutive to a very long evaporation chain starting in the actinide region. The fact that the light evaporation residues are not depopulated in the uranium case compared to the lead one indicates that the fission probability along the extensive de-excitation path is rather low. Regarding Figure 9, this rather astonishes considering that this path crosses the actinide and pre-actinide regions, where the fission barriers are low. The explanation lies in the inhibition of the fission process for very highly excited nuclei. Indeed, the nuclear fission is a dynamical process, which needs time. In a macroscopic picture of the nucleus, Grangé and Weidenmüller [18], following the pioneering work of Kramers [19], treated the fission as a diffusive process over a potential barrier. Considering this approach, the fission process needs the coupling between intrinsic and collective excitation in order to proceed. This coupling is the viscosity. They treated the problem solving the Fokker-Planck equation numerically. At this time, the lack of experimental data did not allow to fix a value for the coupling parameter, the dissipation coefficient that is related to the viscosity of nuclear matter. Recent efforts have been performed for determining this constant. The present data will contribute to this aim.

Thus, we noticed that the fission seems to be inhibited for highly excited nuclei (more than a couple of hundreds MeV of excitation energy). In such a case, the typical de-excitation times are rather short, always much shorter than the time needed for equilibrating the fission-degree of freedom. Consequently, the fission channel is not open for highly excited actinides. When the nucleus cools down, emitting nucleons and light charged particles, the typical emission time increases, allowing the fission process to occur. However, the fission barriers become also higher in the pre-actinide region reducing the fission widths.

The isotopic distributions of the cross sections in the fission region for the system $^{238}U + ^{1}H$ shown on Figure 5 are characterized by a wide Gaussian shape, modified by a shoulder on the n-rich side for elements Z = 50 to 58. This component reflects the high fission probability at low excitation energies of ^{238}U and its neighbours, giving the most neutron-rich isotopes. Governed by the asymmetric fission mode, this contribution disappears for symmetric break-up of uranium, around Z = 46, where an almost perfect Gaussian shape is observed in the case of rhodium, palladium and silver. This contribution is seen in the Z distribution (Figure 10) as well, with enhanced values compared to a Gaussian shape for Z between 50 to 58. The mean value of the fission-fragment nuclear-charge distribution is 44.1 and its variance is 6.6 charge units. Other characteristic features of the spallation-fission distributions are the mean N-over-Z ratio and the width of the isotopic distributions, also shown in Figure 10.

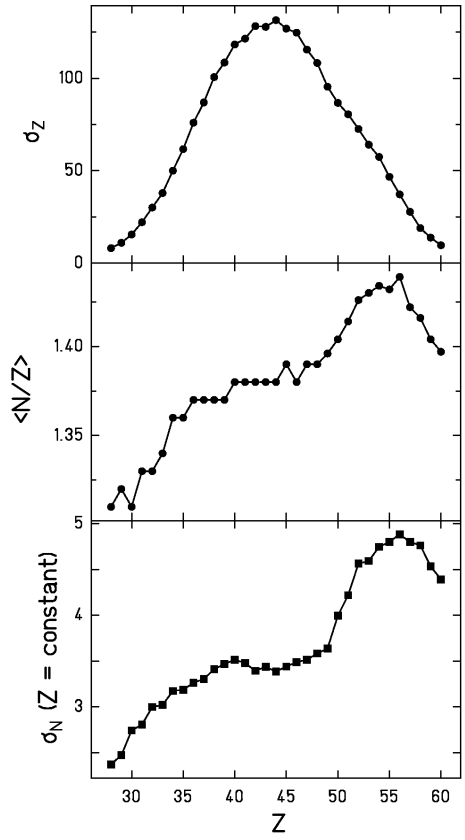

Figure 10 : Measured fission-fragment element distribution (upper part), mean neutron-to-proton ratio (central part) and width of the isotopic distributions (lower part).

Measured fission cross sections extend far down to values as low as 0.01 mb on the neutron-rich side, since there is no contribution from secondary reactions in this region. At the other end, in the region of n-deficient fragments a contribution of secondary products prevents to reach such a sensitivity.

At the present stage of the data analysis, the spallation-evaporation cross section for ^{238}U + ^{1}H at 1 *A* GeV amounts to about 460 mb, while the fission cross section is found to be about 1.3 b, which agrees with the most recent data evaluation [20]. The spallation-evaporation cross section for ^{238}U + ^{2}H at 1 *A* GeV amounts to about 825 mb, 705 mb measured for $Z \geq 65$ and 120 mb estimated below this limit, while the fission cross section is found to be about 1.2 b between Z = 23 and Z = 60. As can be seen in Figure 6 and Figure 7, the spallation-evaporation residues produced in the deuteron-induced reaction reach to lower masses, which are less fissile than the heavier ones produced in the proton-induced reaction. Therefore, the fission cross section slightly decreases in the deuteron-induced reaction compared to the proton-induced reaction, while the expected increase of the total reaction cross section is found in the spallation-evaporation residues. Summing up the different components, the measured total reaction cross sections are somewhat lower than calculated with Glauber-type calculations [21], which yield 1.96 b for ^{238}U + ^{1}H and 2.51 b for ^{238}U + ^{2}H.

3.2 Velocity distribution

The experimental set up allows determining the recoil-velocity properties of the produced nuclei. In this section, we present the results for the system $^{238}U + ^{1}H$. The values for the system $^{238}U + ^{2}H$ turned out to be rather similar.

For the spallation-evaporation residues, the velocity distributions are well represented by Gaussian distributions. We could determine the mean value and the standard deviation of the recoil-velocity distribution for each ions. We accounted for the slowing down in the target area, assuming that the nuclear reaction occurred in the middle of the target on the average.

We plotted in Figure 11 the mean velocity normalised following the prescriptions of Morrissey [22]. Thus, we introduce $p'_{||}$, which is the longitudinal recoil momentum, normalized in the following way:

$$p'_{||} = v_{||}^{*} M_p^{*} (\beta\gamma/(\gamma+1)) \quad (6)$$

Here, $v_{||}^{*}$ is the velocity of the fragment in the frame of the projectile, and M_p^{*}, β and γ are the mass and the relativistic parameters of the projectile in the laboratory frame, respectively.

This normalisation allows an inter-comparison of various measurements realised at different projectile energies. The location straggling is also unfolded for estimating the standard deviation of the velocity distribution. Note, however, that this contribution is negligible in the present experiment. Figure 11 also includes the empirical systematics stated by Morrissey [22], which predicts a linear dependence between the reduced recoil momentum ($p'_{||}$) and the mass loss (relative to the mass of the projectile). We observe that the systematics describes reasonably well the measured data. However, there are two remarkable differences. Firstly, the measured data are systematically lower over the whole mass range. Secondly, there is a dependency on the neutron excess in the isotopic chains close to the projectile, which cannot be seen Figure 11, since these values are averaged over the whole chain: The momentum width decreases with increasing neutron excess. This variation is traced back to the variation of the contribution of evaporation to the mass loss as observed previously in slightly lighter systems [16, 23].

The width of the longitudinal recoil momentum acquired in the spallation-evaporation reaction is shown in Figure 12. Again, the data are compared with the systematics of Morrissey, and also with the predictions of the Goldhaber model [24]. While the systematics better represents the data for mass losses below $\Delta A = 20$, the experimental values increase more strongly for large mass losses and reach the prediction of the Goldhaber model for $\Delta A \approx 55$. Also in the width of the momentum distribution, isotopic variations are observed which are related to the variation of the evaporation contribution to the mass loss [23].

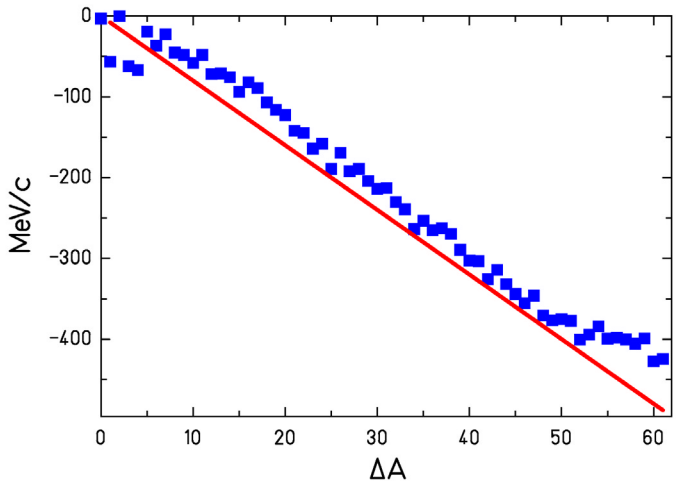

Figure 11 : Mean recoil momentum induced in the spallation of ^{238}U by 1 GeV protons as a function of mass loss. The data (symbols) are compared with the systematics of Morrissey [22]. Since the measurement has been performed in inverse kinematics, the measured momenta are transformed into the frame of the beam.

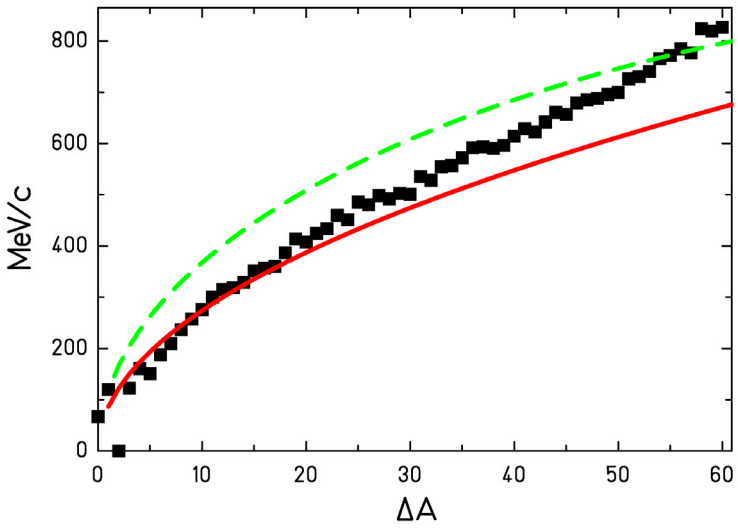

Figure 12 : Standard deviation of the longitudinal momentum distribution of the spallation-evaporation residues produced in the bombardment of ^{238}U with 1 GeV protons. The data (symbols) are compared with the Goldhaber model [24] (dashed line) and with the Morrissey systematics [22] (full line). Since the measurement has been performed in inverse kinematics, the measured momenta are transformed into the frame of the beam.

The velocities of the lighter and the heavier fission fragments are reported in Figure 13 and Figure 14, respectively. Figure 13 separately gives the velocities of the fission fragments emitted in forward and backward direction and in addition the mean velocity of the fissioning system. Obviously, the fissioning system has acquired a slightly negative momentum in the preceding intra-nuclear cascade stage. The velocities acquired in the fission process correspond to half the difference of the values given for the fragments emitted in forward and backward directions. These fission velocities are shown in Figure 14 for the heavier group of

the fission fragments. All fission velocities are consistent with the binary decay of a heavy nuclear system between lead and uranium. The strong variation of the fission velocity with the atomic number of the fission fragment is mostly given by momentum conservation.

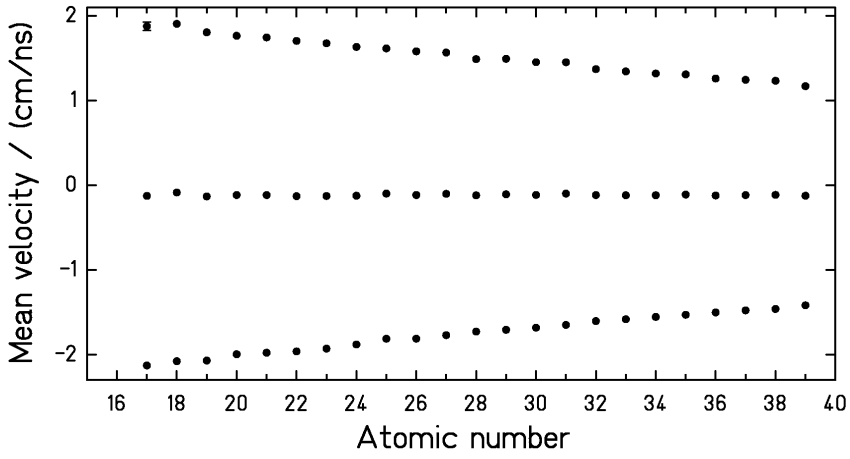

Figure 13 : Upper and lower symbols : Mean velocities of light fission products emitted in forward and backward direction, formed after the spallation of ^{238}U by 1 GeV protons. Central symbols: Mean velocity of the fission products. Since the measurement has been performed in inverse kinematics, the velocities are transformed into the frame of the beam.

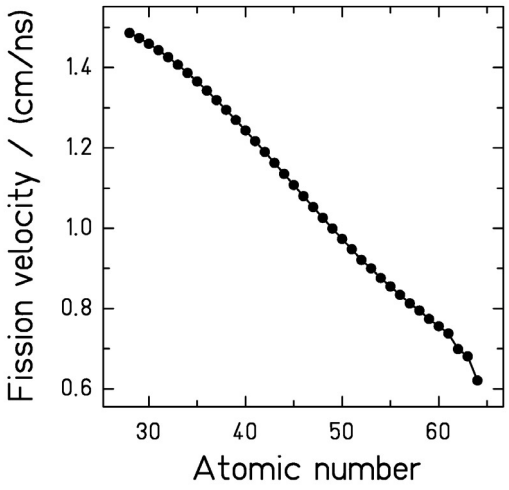

Figure 14 : Velocity of the fission fragments produced in the spallation-fission reaction of ^{238}U induced by 1 GeV protons as a function of the atomic number of the fission fragments. Since the measurement has been performed in inverse kinematics, the velocities are transformed into the frame of the beam.

3.3. Comparison to other data

We could find very few results which can be compared to ours. Actually, three different experiments matched to the present one for proton-induced spallation-evaporation reactions. Lindner and Osborne [25] studied the evaporation-residue production after the spallation of ^{238}U by 340 MeV protons, Pate and Poskanzer [26] studied the same reaction at 680 MeV. The projectile energy is sensibly lower, but we expect little variations due to the projectile energy modification for the heaviest fragments. They experimentally irradiated the uranium

target and applied chemical techniques followed by a spectroscopic analysis. Titarenko and collaborators [27, 28] also measured several evaporation residues produced by the same reaction at 800 MeV. They used pure spectroscopic methods. In such cases, the experimental technique authorises measuring independent yields of protected nuclei, this means, nuclei, which are not produced by the decay of any potential mother isotopes.

Figure 15 compares the various cross sections obtained by Lindner and Osborne [25], by Pate and Poskanzer [26] and by Titarenko and collaborators [27, 28] to the present data.

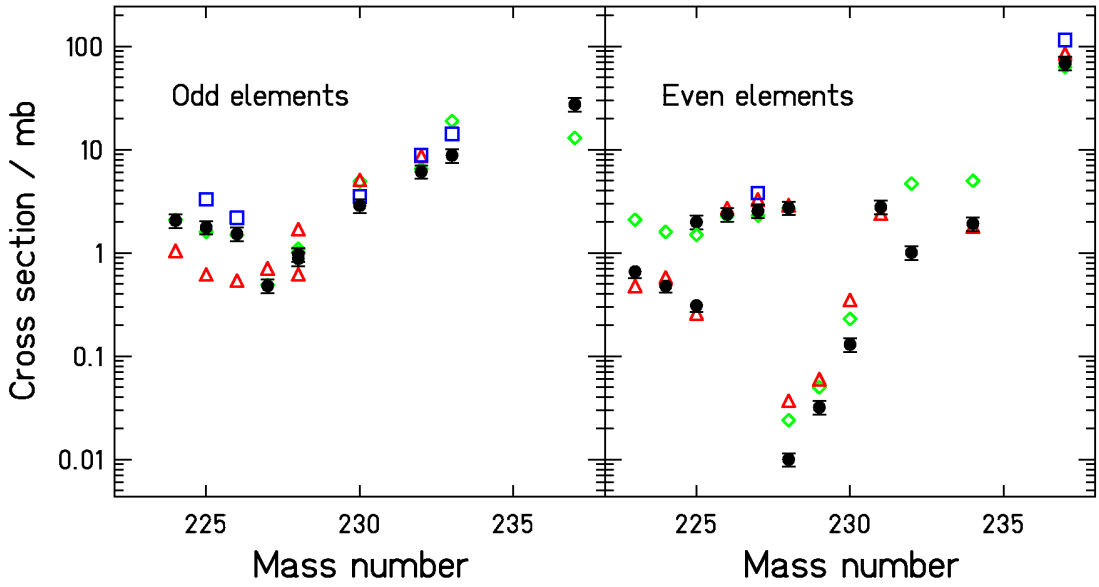

Figure 15 : Comparison of the spallation-evaporation cross sections determined in this work with previous results obtained by gamma spectroscopic methods for ^{237,232,230,229,228}U, ^{234,231,228,227,226,225}Th, ^{225,224,223}Ra (upper part) and ^{237,233,232,230,228,227}Pa, ^{228,226,225,224}Ac (lower part) from refs. [25] (triangles), [26] (diamonds), and [27, 28] (squares).

We observe a systematic disagreement between our data and the ones from Titarenko and collaborators. They systematically overestimate the cross sections in comparison to ours. On the other hand, many of the data obtained by Lindner and Osborne nicely fit to our results, others, especially the lower cross sections, deviate by up to a factor of 3 in both directions. Also many data of Pate and Poskanzer agree with our values, while others, in particular those for thorium and uranium isotopes, are considerably higher. Most of the deviations between the different measurements are not systematic. It seems that the older measurements suffer from some normalisation problems for specific elements, while a large number of data is in very good agreement with our results. Only the data of Titarenko et al. are all somewhat higher that ours.

We have no explanation for the systematic discrepancy between our data and the ones of Titarenko and collaborators. However, we remark that we applied the same procedure than that which was followed for studying the spallation of gold and lead at a similar energy. For those experiments, the normalisation was ensured since the sum of the measured evaporation residues and fission fragment production yielded the total inelastic cross section which has been determined with high precision in previous experiments.

For spallation-fission residues, the comparison with previous data is possible only in case of alkaline fragments, which were investigated with on-line mass-separation techniques [29]. These data on complete isotopic distributions for two elements, rubidium and caesium are compared with the new results of this work in Figure 16. In perfect agreement in case of rubidium isotopes, our results show a discrepancy for the Cs isotopic distribution. We obtain lower values for intermediate and low masses. This difference cannot be explained by secondary reactions which are expected to depopulate mostly neutron-rich species.

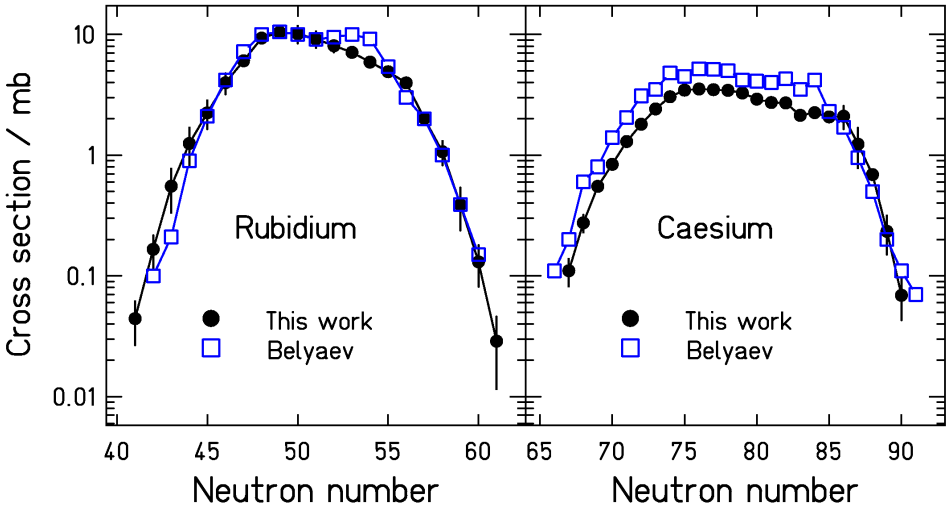

Figure 16 : Comparison of the spallation-fission cross sections of rubidium and caesium isotopes obtained in this work with previous results [29].

Several nuclides have also been investigated extensively at ISOLDE, CERN. It was not the aim of these experiments to measure the production cross sections, but in a few cases the yields have systematically been determined for long isotopic chains [30]. Since no information on the reaction kinematics was available for the spallation reaction in a thick target, the reaction process was not known. At that time, the production of light residues below elements populated in low-energy fission ($Z < 25$) was attributed to a kind of "fragmentation". We now know by the measured velocities (see Figure 4) that these nuclei are produced by fission.

In Figure 17, we compare the production cross sections of potassium isotopes with the yields obtained at ISOLDE. Although this comparison cannot be made on an absolute scale, the two curves seem to join nicely. The slight shift in the maximum might be caused by the different beam energies of the two measurements and by secondary production in the ISOLDE target. For the higher beam energy used in our experiment, the excitation energy and hence the neutron evaporation is increased, leading to enhanced production of neutron-deficient isotopes. The systematics of the cross sections (Figure 6) and the velocity distributions (Figure 13) of our experiment reveals that light nuclei down to oxygen are produced in the spallation of ^{238}U by 1 GeV protons as a tail of the fission distribution. The lightest products, however, appear in a transition region between fission and evaporation, which are anyhow to be considered as a common process of binary decay with gradually varying properties.

4. Conclusion

A total number of 2509 individual nuclide production cross sections and velocity distributions in the reactions of 1 *A* GeV ^{238}U with hydrogen and deuterium have been studied, covering most elements between nitrogen and uranium. The reaction products were fully identified in atomic number *Z* and mass number *A* using the magnetic spectrometer FRS. Moreover, the velocity distribution of each individual nucleus was measured.

The data, production cross sections and kinetic energies, are of highest interest for the design of accelerator-driven systems. Using the measured production cross sections, combined with the known decay properties, the short- and long-term radioactivities in irradiated fissile material can be calculated. The systems investigated provide stringent constraints to nuclear-reaction codes, in particular to the modelling of the fission competition and the nuclide production in fission. The new data will help to develop improved models with better predictive power for spallation reactions involving highly fissile nuclei.

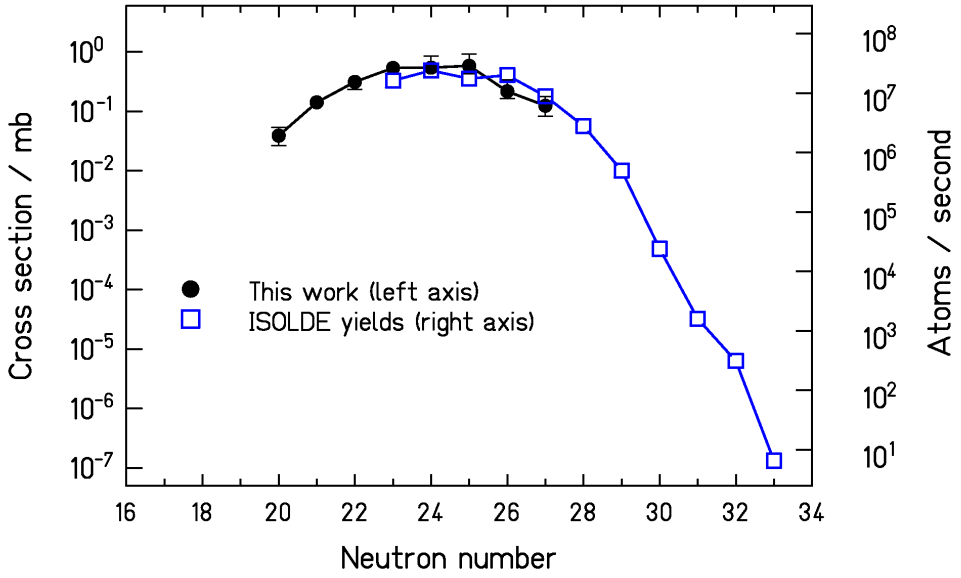

Figure 17 : Comparison of the spallation-fission cross sections of potassium isotopes determined in this work (left scale) with yields obtained at ISOLDE in the spallation of uranium with 600 MeV protons [30] (right scale).

The data are also highly relevant for the design of next-generation radioactive-beam facilities, since they give a first systematic overview on the characteristics of the production of radioactive nuclear beams in spallation reactions. These data are of particular interest for the planning of ISOL-type facilities, where the production of rare isotopes is based on spallation reactions.

Mass distributions of spallation-evaporation residue of the present work were compared with results of similar experiments on ^{197}Au (0.8 *A* GeV) and ^{208}Pb (1 *A* GeV) on hydrogen. The comparison reveals the strong influence of the fission competition in the uranium system.

The comparison of our results with the scares existing data demonstrates the important progress brought about by the inverse-kinematic technique which allows to measure and uniquely identify essentially all residues prior to their radioactive decay down to half-lives in the range of microseconds.

References

[1] "Measurement of isotopic cross sections of spallation residues in 800 A MeV ^{197}Au + p collisions"
F. Rejmund, B. Mustapha, P. Armbruster, J. Benlliure, M. Bernas, A. Boudard, J. P. Dufour, T. Enqvist, R. Legrain, S. Leray, K.-H. Schmidt, C. Stéphan, J. Taïeb, L. Tassan-got, C. Volant
Nucl. Phys. **A 683** (2001) 540-565

[2] "Isotopic production cross sections of fission residues in ^{197}Au-on-proton collisions at 800 A MeV "
J. Benlliure, P. Armbruster, M. Bernas, A. Boudard, J. P. Dufour, T. Enqvist, R. Legrain, S. Leray, B. Mustapha, F. Rejmund, K.-H. Schmidt, C. Stéphan, L. Tassan-Got, C. Volant
Nucl. Phys. **A 683** (2001) 513-539

[3] "Cross sections of spallation residues produced in 1 A GeV ^{208}Pb-on-proton reactions "
W. Wlazlo, T. Enqvist, P. Armbruster, J. Benlliure, M. Bernas, A. Boudard, S. Czajkowski, R. Legrain, S. Leray, B. Mustapha, M. Pravikoff, F. Rejmund, K.-H. Schmidt, C. Stephan, J. Taïeb, L. Tassan-Got, C. Volant
Phys. Rev. Lett. **84** (2000) 5736

[4] "Isotopic yields and kinetic energies of primary residues in 1 A GeV ^{208}Pb + p reactions"
T. Enqvist, W. Wlazlo, P. Armbruster, J. Benlliure, M. Bernas, A. Boudard, S. Czajkowski, R. Legrain, S. Leray, B. Mustapha, M. Pravikoff, F. Rejmund, K.-H. Schmidt, C. Stéphan, J. Taïeb, L. Tassan-Got, C. Volant
Nucl. Phys. **A 686** (2001) 481-524

[5] "Primary residue production cross sections and kinetic energies in 1 A GeV ^{208}Pb-on-deuteron reactions "
T. Enqvist, P. Armbruster, J. Benlliure, M. Bernas, A. Boudard, S. Czajkowski, R. Legrain, S. Leray, B. Mustapha, M. Pravikoff, F. Rejmund, K.-H. Schmidt, C. Stéphan, J. Taïeb, L. Tassan-Got, F. Vivès, C. Volant, W. Wlazlo
Nucl. Phys. **A 703** (2002) 435-465

[6] "The GSI projectile fragment separator (FRS) – a versatile magnetic system for relativistic heavy ions"
H. Geissel, P. Armbruster, K.-H. Behr, A. Brünle, K. Burkard, M. Chen, H. Folger, B. Franczak, H. Keller, O. Klepper, B. Langenbeck, F. Nickel, E. Pfeng, M. Pfützner, E. Roeckl, K. Rykaczewsky, I. Schall, D. Schardt, C. Scheidenberger, K.-H. Schmidt, A. Schröter, T. Schwab, K. Sümmerer, M. Weber, G. Münzenberg, T. Brohm, H.-G. Clerc, M. Fauerbach, J.-J. Gaimard, A. Grewe, E. Hanelt, B. Köedler, M. Steiner, B. Voss, J. Weckenmann, C. Ziegler, A. Magel, H. Wollnik, J.-P. Dufour, Y. Fujita, D. J. Vieira, B. Sherrill
Nucl. Instrum. Methods **B 70** (1992) 286-297

[7] "Liquid hydrogen target for cross-section measurements relevant for nuclear-waste incineration"
P. Chesney, A. Forgeas, J. M. Gheller, G. Guiller, P. Pariset, L. Tassan-Got, P. Armbruster, K.-H. Behr, J. Benlliure, K. Burkard, A. Brünle, T. Enqvist, F. Farget, K.-H. Schmidt
GSI Ann. Rep. 97-1 (1996) 190

[8] J. Taïeb, PhD thesis, IPN Orsay, France

[9] E. Casarejos, PhD thesis, Univ. Santiago de Compostela, Spain

[10] M. Bernas, private communication

[11] M. V. Ricciardi, PhD thesis, in preparation

[12] J. Pereira, PhD thesis, in preparation
[13] "First spatial isotopic separation of relativistic uranium projectile fragments "
A. Magel, H. Geissel, B. Voss, P. Armbruster, T. Aumann, M. Bernas, B. Blank, T. Brohm, H.-G. Clerc, S. Czajkowski, H. Folger, A. Grewe, E. Hanelt, A. Heinz, H. Irnich, M. de Jong, A. Junghans, F. Nickel, M. Pfützner, A. Piechaczek, C. Röhl, C. Scheidenberger, K.-H. Schmidt, W. Schwab, S. Steinhäuser, K. Sümmerer, W. Trinder, H. Wollnik, G. Münzenberg
Nucl. Instr. Methods **B 94** (1994) 548-554
[14] "Projectile-fragment yields as a probe for the collective enhancement in the nuclear level density "
A. R. Junghans, M. de Jong, H.-G. Clerc, A. V. Ignatyuk, G. A Kudyaev, K.-H. Schmidt
Nucl. Phys. **A 629** (1998) 635-655
[15] "Application of a Secondary-Electron Transmission Monitor for High-Precision Intensity Measurements of Relativistic Heavy-Ion Beams"
B. Jurado , K.-H. Schmidt, K.-H. Behr
Nucl. Instrum. Methods **A** (2002) 603-610
[16] B. Mustapha, PhD thesis, IPN Orsay
[17] "Production of neutron-rich isotopes by cold fragmentation in the reaction ^{197}Au + Be at 950 *A* MeV"
J. Benlliure, K.-H. Schmidt, D. Cortina-Gil, T. Enqvist, F. Farget, A. Heinz, A. R. Junghans, J. Pereira, J. Taïeb
Nucl. Phys. **A 660** (1999) 87-100
[18] "Fission probability and the nuclear friction constant"
P. Grangé, H. A. Weidenmüller
Phys. Lett. **B 96** (1980) 26-30
[19] "Brownian motion in a field of force and the diffusion model of chemical reactions"
H. A. Kramers
Physica **7** (1940) 284-304
[20] "Compilation and systematics of proton-induced fission cross-section data"
A. V. Prokofiev
Nucl. Instrum. Methods **A 463** (2001) 557-575
[21] "Nucleus-nucleus reaction cross sections at high energies: soft spheres model "
P. J. Karol
Phys. Rev. **C 11** (1975) 1203-1209
[22] "Systematics of momentum distributions from reactions with relativistic ions"
D. J. Morrissey
Phys. Rev. **C 39** (1989) 460-470
[23] "Momentum distributions of projectile fragments produced in the cold and hot fragmentation of relativistic ^{136}Xe and ^{197}Au projectiles "
E. Hanelt, A. Grewe, K.-H. Schmidt, T. Brohm, H.-G. Clerc, M. Dornik, M. Fauerbach, H. Geissel, A. Magel, G. Münzenberg, F. Nickel, M. Pfützner, C. Scheidenberger, M. Steiner, K. Sümmerer, B. Voss, M. Weber, J. Weckenmann, C. Ziegler
Z. Phys. **A 346** (1993) 43-46
[24] "Statistical models of fragmentation processes"
A. S. Goldhaber
Phys. Lett. **B 53** (1974) 306-308
[25] "Nonfission inelastic events in uranium and thorium induced by high-energy protons "
M. Lindner, R. N. Osborne
Phys. Rev. **103** (1956) 378

[26] "Spallation of uranium and thorium nuclei with BeV-energy protons“
B. D. Pate, A. M. Poskanzer
Phys. Rev. **123** (1961) 647
[27] Y. Titarenko O. V. Shvedov, VYachaslev F. Batyaev, Eugeny I. Karpikhin, Valery M. Zhivun, Aleksander B. Koldobsky, Ruslan D. Mulambetov, Andrey N. Sosnin, Yuri, N. Shubin, Anatoly V. Ignatyuk, Vladimir P. Lunev, Stepan G. Mashnik, Richard E. Prael, Tony A. Gabriel, Marshall Blann, 3rd international conference on accelerator driven transmutation technologies and applications (Prague – Czech Republic), June 1999.
[28] Y. Titarenko, Private Communication, August 2000
[29] "Rb and Cs isotopic distributions from 1 GeV proton fission of ^{238}U"
B. N. Belyaev, V. D. Domkin, Yu. G. Korobulin, L. N. Androneko, G. E. Solyakin
Nucl. Phys. **A 348** (1980) 479-492
[30] User guide ISOLDE, CERN, Geneva, H.-J. Kluge ed.